Applied Catalysis B: Environmental 168-169 (2015) 125–131

Contents lists available at ScienceDirect

Applied Catalysis B: Environmental

journal homepage: www.elsevier.com/locate/apcatb

Photocatalytic reduction of CO_2 with water vapor on surface La-modified TiO_2 nanoparticles with enhanced CH_4 selectivity

Ying Liu [a], Sheng Zhou [a], Jianmei Li [a], Yajun Wang [a], Guiyuan Jiang [a,**], Zhen Zhao [a,*], Bing Liu [a], Xueqing Gong [b], Aijun Duan [a], Jian Liu [a], Yuechang Wei [a], Liqiang Zhang [a]

[a] State Key Laboratory of Heavy Oil Processing, China University of Petroleum, Beijing 102249, China
[b] State Key Laboratory of Chemical Engineering, East China University of Science and Technology, Shanghai 200237, China

ARTICLE INFO

Article history:
Received 25 August 2014
Received in revised form 3 December 2014
Accepted 7 December 2014
Available online 12 December 2014

Keywords:
Surface La modification
La_2O_3
Semiconductors
Photocatalytic reduction of CO_2
CH_4 formation

ABSTRACT

Surface La-modified TiO_2 nanoparticle samples were prepared by a simple sol–gel method. The structure and properties of the catalysts were characterized and analyzed by means of XRD, TEM, BET, UV–vis DRS, CO_2-TPD, XPS, Raman and Theoretical Calculation. The most La^{3+} was found to deposit onto the TiO_2 in the form of La_2O_3 particles, and a tiny number of La atoms modify TiO_2 by substituting the surface Ti atom in the form of Ti—O—La, leading to the generation of oxygen vacancies and Ti^{3+} for balancing the charge. The La-modified TiO_2 photocatalysts were investigated in the photocatalytic reduction of CO_2 with water vapor under the 300 W Xe arc lamp irradiation. The La-modified TiO_2 showed high CH_4 yield of 3.457 μmol under 20 h light irradiation, which is 13 times of that over commercial P25. The enhanced photocatalytic performances were attributed to the synergistic effects of basic characteristics of La_2O_3 for CO_2 adsorption, the oxygen vacancies for water vapor activation and Ti^{3+} for electron separation.

1. Introduction

Since the first demonstration of photocatalytic reduction of CO_2 to organic compounds in 1979 by Inoue et al. [1], the research on photocatalytic conversion of CO_2 has been received increasing attention because it offers an ideal option for the utilization of renewable energe and solving the related environmental problems [2–5]. The design and development of efficient photocatalyst that combines CO_2 activation and the subsequent photocatalysis is the key to this process. Among the various photocatalysts that have been studied for CO_2 photoreduction, TiO_2 is a promising candidate in terms of its strong redox ability, low cost, stability, and environmental friendliness [6–8]. However, TiO_2 as photocatalyst suffers from some disadvantages that lead to low reaction efficiency [9]. The major challenges are its wide band gap (~3.2 eV for anatase and 3.0 eV for rutile), recombination of photo-induced electron–hole, and uncontrolled photoselectivity [10]. In order to improve the photocatalytic performances of TiO_2, many strategies have been proposed, including the loading of metals (e.g., Pd, Rh, Pt, Ag, and Cu) [11–15], metal oxides (e.g., Cu_2O, CeO_2, and MgO) [16–20], and doping non-metal ions (e.g., N and I) [21–24], etc.

Among various modifications of TiO_2, the use of basic oxide in improving CO_2 photoreduction has attracted a great deal of attention. Basic oxide has been proposed to promote the CO_2 adsorption and destabilize CO_2 molecules [24,25], and as the insulator it could facilitate separation of the photogenerated electrons and holes [19]. Xie et al. [20] suggested that some basic oxides undermine the stability of CO_2 molecules, enhance the density of destabilized CO_2 molecules on the catalyst surface, and promote the formation of CH_4. Rare earth oxide is a typical and widely investigated oxide, besides the reports on using the basic properties of some rare earth oxides, studies have also shown that the use of rare earth elements for TiO_2 modification could extend the adsorption region, prevent the transformation phase of TiO_2 from anatase to rutile [26], and increase the surface oxygen vacancies [27], etc. Results from Matějová et al. [28] indicate that the addition of Ce atoms in TiO_2 not only changes the spectral response, but also affects the energies of electrons and holes of the catalysts, thereby enhancing the CO_2 photoreduction activity. So, the introduction of rare earth elements or their oxides into the classic semiconductor photocatalysts are expected to utilize both the basic property for CO_2 activation and their unique effects on the regulation of light response and other properties. However, rare earth-modified TiO_2 mostly adopts the direct loading mode. Up to now, there are few reports on the

* Corresponding author. Tel.: +86 10 8973 1586; fax: +86 10 6972 4721.
** Corresponding author. Tel.: +86 10 8973 9125; fax: +86 10 6972 4721.
E-mail addresses: jianggy@cup.edu.cn (G. Jiang), zhenzhao@cup.edu.cn (Z. Zhao).

http://dx.doi.org/10.1016/j.apcatb.2014.12.011
0926-3373/

simultaneous introduction of the rare earth oxides and rare earth element modification, not mentioning the application in the photoreduction of CO_2.

In this study, we report the synthesis of the La_2O_3-modified TiO_2 with in-situ surface modification of La by a simple sol–gel method, and their catalytic performances for photoreduction of CO_2 with water vapor. The as-prepared catalysts demonstrated the enhanced selectivity to CH_4. Based on the characterization and the photocatalytic results, the mechanism for the photoreduction of CO_2 with H_2O vapor on the as-prepared photocatalyst was also proposed.

2. Experimental

2.1. Materials

All the chemicals were used as purchased without further purification: Tetra-n-butyl titanate ($Ti(OBu)_4$, ≥98.0%) and Lanthanum(III) Oxide (La_2O_3, 99.99%) were purchased from Sinopharm Chemical Reagent Co., Ltd., Nitric acid (HNO_3, 65.0–68.0 wt/%) was purchased from Beijing Chemical Works. P25 was purchased from Germany Degussa Co., Ltd. Anhydrous ethanol ($C_2H_5OH \geq 99.7\%$) was purchased from Beijing Modern Oriental Fine Chemistry Co., Ltd.

2.2. Preparation of catalysts

The La-modified TiO_2 nanoparticles were prepared by a sol–gel method with $Ti(OBu)_4$ as the titanium source [29]. 10 mL of $Ti(OBu)_4$ was dissolved in 40 mL of anhydrous ethanol in a dry atmosphere, and then the mixed solution of $Ti(OBu)_4$ and ethanol was added dropwise into another mixture solution consisting of 10 mL water, 10 mL of anhydrous ethanol, and a certain amount of La_2O_3 dissolved in 2 mL of 70% HNO_3 under vigorous stirring. 0 #, 1 #, 2 #, 3 #, 4 # and 5 # denote the samples in which the molar ratio of La to Ti was 0, 0.01, 0.02, 0.03, 0.04, 0.05, respectively, during catalyst preparation. Subsequently, the mixed solution was stirred in a closed beaker at room temperature for 3 h to carry out further hydrolysis. Then, the yellowish transparent sol was obtained, which was aged for 6 h at room temperature and dried at 343 K for 36 h in air to remove water and alcohol for getting a xerogel. Finally, TiO_2 nanoparticles were obtained by calcination of TiO_2 xerogel at the 873 K in air for 2 h with subsequent grinding.

2.3. Sample characterization

To characterize the crystal structure of the catalysts, powder X-ray diffraction (XRD) patterns were recorded with a diffractometer (Shimadzu XRD 6000) using Cu Kα ($\lambda = 0.15406$ nm) radiation with a Nickel filter operating at 40 kV and 10 mA. The Brunauer–Emmett–Teller (BET) specific surface area of the samples were analyzed by nitrogen adsorption at 77 K on Micromeritics ASAP 2020 analyzer and calaulated by the Brunauer–Emmett–Teller (BET) method. Images of transmission electron microscopy (TEM) and high resolution transmission electron microscopy (HRTEM) were obtained with a JEOL JEM-2100 electron microscope equipped with a field emission source at an accelerating voltage of 120 kV. Image of aberration-corrected high resolution transmission electron microscopy was got on a FEI Titan 80-300 equipped with a spherical aberration corrector for objective lens. The UV–vis diffused reflectance spectra (DRS) experiments were performed on a UV–vis spectrophotometer (Hitachi U-4100) using BaSO4 as the background. The surface chemical states and atomic concentration were characterized by X-ray photoelectron spectroscopy (XPS) and the measurements were performed on PerkinElmer PHI-1600 ESCA spectrometer using MgKα ($h\nu = 1253.6$ eV, 1 eV = 1.603×10^{-19} J) X-ray source. The XPS spectrum was calibrated with respect to the binding energy of the C 1s peak at 284.6 eV and was deconvoluted using related software. Electron paramagnetic resonance (EPR) was carried out at room temperature on an instrument JES FA-200 (JEOL) operating at the band frequency about 10.0 GHz with a field modulation frequency of 100 kHz. The modulation width was set at 0.1 mT and used microwave power was 1 mW. Visible Raman spectra were recorded at room temperature on a Renishaw Invia scanning double monochromator with the spectral resolution of 4 cm^{-1}. The line at 532 nm single-frequency laser was used as the excitation source. The ^{13}C isotopic tracer experiments were conducted and the obtained photocatalytic products were identified by a Thermo Fisher DSQ system. Such a GC–MS was equipped with a HP-5MS (30 m × 0.25 mm × 0.25 μm) fused silica capillary column. The mass spectrometer was operated with an electron impact (EI) source at 70 eV ionization energy and scanned from 10 to 150 amu.

2.4. CO_2 temperature-programmed desorption (CO_2-TPD)

CO_2 temperature-programmed desorption experiments were carried out using a Quantachrome Autosorb-IQ which consists of a flow switching system, a heated reactor, and a mass spectrometer. The samples (200 mg) were loaded in the reactor.

Before the TPD analysis, the sample was purged under helium flow (50 mL min^{-1}) from room temperature up to 873 K for 60 min at a heating rate of 10 K min^{-1}. The sample was subsequently cooled to 323 K under He flow, then the He flow was switched to CO_2 maintaining for 60 min. And then, the sample was swept with He for 100 min. The temperature was increased at 10 K min^{-1} from 323 to 1173 K. The 44, 35, 28, and 18 mass numbers were monitored during the TPD experiments.

2.5. Theoretical calculation

All the theoretical calculations were performed using the Vienna ab-initio simulation package (VASP) with the employment of a plane wave basis set [30]. To analyze electron correlations in transition metal oxides, we conducted spin-polarized DFT+U calculations with a value of $U = 4.0$ eV applied to the Ti atom. The projector-augmented wave (PAW) method was used to represent the core-valence interaction [31]. The plane wave energy cutoff was set to 400 eV. The generalized gradient approximation (GGA) with the Perdew–Burke–Ernzerhof (PBE) exchange-correlation functional was used in the calculations [32]. Gaussian smearing method with the width of 0.05 eV was used. The Brillouin zone was sampled at the Γ-point. The convergence criteria for the energy and force were set to 10^{-5} eV and 0.02 eV/Å, respectively.

A slab model of anatase TiO_2(1 0 1) surface was used in this study. The optimized lattice parameters of bulk anatase TiO_2 structure are $a = 3.78$, $b = 3.78$, and $c = 9.49$. This TiO_2 model contains 72 atoms, with 48 O atoms and 24 Ti atoms. A vacuum gap of 12 Å was employed in this study. During geometry optimization, all the atoms were allowed to relax. The La-modified TiO_2 was modeled by replacing one Ti atom with one La atom in the surface layer of anatase TiO_2(1 0 1).

2.6. Photocatalytic CO_2 reduction

The photocatalytic CO_2 reduction reactions were carried out in LabSolar-H2 system, and the schematic of experimental system is shown in Fig. S1. 100 mg La-modified TiO_2 catalyst was well-distributed onto a groove of circular glass reactor with an inner basal area of 20 cm^2. A 300 W Xe arc lamp was used as a light source without use of filter. Light passed through a thickness of 6 cm IR water filter, and then the filtered light was focused onto the reactor. All samples were tested under UV–vis irradiation for 12 h. Degussa

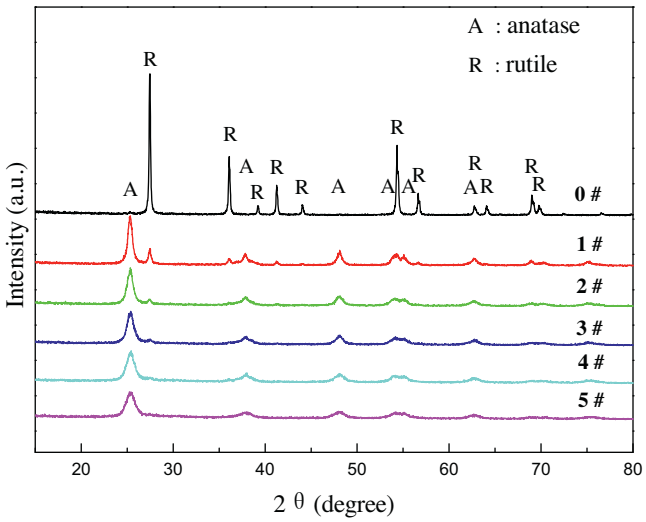

Fig. 1. (a) XRD patterns of 0 #, 1 #, 2 #, 3 #, 4 # and 5 # samples.

P25 and pure anatase were selected as the reference catalysts in photoreduction of CO_2. The reaction setup was vacuumed and full of high purity CO_2 gas several times, and finally the CO_2 and water vapor mixture was bubbled into the reaction setup until reaching ambient pressure, the mixture gas regulated by CO_2 was passed through the water of constant temperature 303 K bubbler to generate the mixture. During irradiation, the photoreduction of CO_2 was operated at closed gas-circulation system and the sampling of gas products for content analysis in the reactor was taken every 1 h by an on-line gas chromatograph (GC-9560 HuaAiSePu Corp., China). The GC-9560 was equipped with two automated gas sampling valves, a thermal conductivity detector (TCD) and two flame ionization detector (FID). The quantification of the products was based on the external standard with the use of a calibration curve.

3. Results and discussion

3.1. Catalyst characterization

The X-ray diffraction (XRD) patterns of pure TiO_2 (0 #) and La-modified TiO_2 (1 #∼5 #) samples are shown in Fig. 1. The peaks marked 'A' and 'R' for samples can be indexed to the anatase and rutile phase of TiO_2, respectively. The pure TiO_2 exhibits the peaks at 27.6°, 36.1°, 41.2°, and 54.3°, which corresponds to the indices of (1 1 0), (1 0 1), (1 1 1), and (2 1 1) planes of rutile phase. For the La-modified TiO_2 samples, with increasing the amount of La, the intensities for the peaks of rutile decrease, while the peaks at 25.5°, 37.9°, 48.2°, 53.8°, and 55.0°, which represent the indices of (1 0 1), (0 0 4), (2 0 0), (1 0 5), and (2 1 1) planes of anatase phase [33] appeared. When the amount of La was increased to 4 mol% (4 #), the peaks corresponding to rutile phase disappeared and the peaks of anatase phase were broadened, indicating that content of La in TiO_2 not only inhibits the phase transformation from anatase to rutile but also avoids the agglomeration of TiO_2 particles [34]. Compared with that of unmodified TiO_2, the particle size of La-modified samples decreases slightly with increasing the content of La, and BET measurement results (Table 1) support this suggestion. Compared with unmodified TiO_2, the specific surface areas of the 5 # samples increased from 3.13 m^2/g to 46.9 m^2/g. Such effects of La loading on samples are in agreement with the literature [34], which is because that the rutile phase formation may start at the defect sites on surface of anatase, and La_2O_3 will easily occupy the defect sites of the anatase particles to prevent the anatase transforming into rutile and the increasing of the grains. Moreover, the XRD did not show any lanthanum oxide phase. It may be due to the very small particle size of lanthanum oxide highly dispersed on the surface layer of TiO_2.

Table 1
The BET surface area, pore size, pore volume and surface atomic ratio of 0 #, 2 # and 5 # samples.

Sample	BET surface area (m^2/g)	BJH pore size (nm)	BJH pore volume (cm^3/g)	Surface atomic ratio of La/Ti (%)
0 #	3.13	9.64	0.01	0
2 #	39.2	10.4	0.09	4.1
5 #	46.9	13.6	0.10	8.4

Fig. 2 shows the TEM and high resolution TEM (HRTEM) images of pure TiO_2, and La-modified samples. As can be seen, the sizes of 0 # and 1 # samples range from 10 to 30 nm (Fig. 2a and b). In comparison, 2 #, 3 #, 4 #, and 5 # samples are uniform with the average particle size of about 10–15 nm (Fig. 2c–f), demonstrating that La modification could inhibit the increase of TiO2 particle size, which is consistent with the results of XRD. The HRTEM image shows the lattice fringe of 0 # sample (Fig. 2g), and the measured interplanar spacing of 0.324 nm corresponds to the (1 1 0) plane of rutile TiO_2. The HRTEM images of 1 # and 2 # samples (Fig. 2h and i) clearly show interplanar spacing of 0.350 nm and 0.249 nm, which confirms the formation of anatase TiO_2 (1 0 1) and rutile TiO_2 (1 0 1), respectively. And 3–5 # samples (Fig. 2j–l) show the measured interplanar spacing of 0.355, 0.241 and 0.19 nm, which correspond to the (1 0 1), (1 0 3) and (2 0 0) plane of anatase TiO_2, respectively. Further characterization from aberration-corrected high resolution transmission electron microscope (Fig. S5) shows that there exists

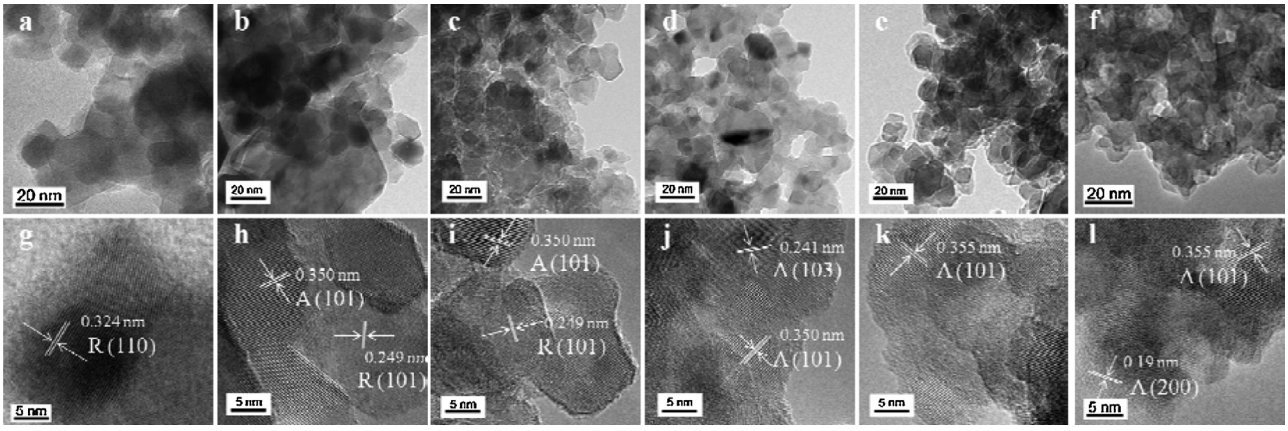

Fig. 2. TEM and HRTEM image of 0 # (a, g), 1 # (b, h), 2 # (c, i), 3 # (d, j), 4 # (e, k), and 5 # (f, l) samples.

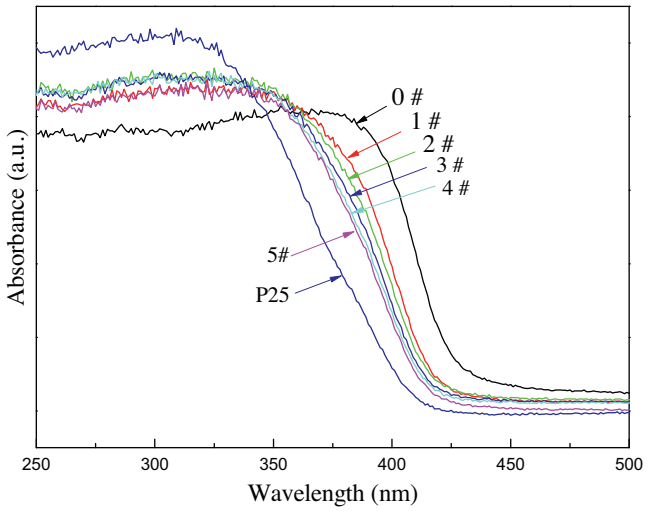

Fig. 3. UV–vis diffuse reflectance spectra of P25 and TiO_2 with different La amount. (0 #–5 #)

La_2O_3 nanoparticle (2 0 1) with the size of 2 ~ 3 nm on the surface of TiO_2.

Fig. 3 shows the UV–vis DRS spectra of P25, pure $TiO_{2(0\,\#)}$, and La-modified TiO_2(1–5 #) catalysts. Compared with P25, all La-modified TiO_2 samples show a red shift of absorption, due to the charge-transfer transition between the *f* electrons of rare earth ion and the conduction or valence band of TiO_2 [26]. The maximum red shift corresponds to pure rutile TiO_2, because of the band gap of TiO_2 is 3.2 eV for anatase and 3.0 eV for rutile. While the absorption of La-modified TiO_2 show obvious blue shift with the increase of La content. This is because that the increase of La content results in the enhanced content of anatase and the decrease of particle size of anatase.

To investigate the interaction of CO_2 and La-modified TiO_2, temperature-programmed desorption of CO_2 was performed. The TPD profiles of CO_2 for 0 # sample, La-modified TiO_2 samples (1–5 #) are shown in Fig. 4. The CO_2 traces (m/e = 44) of the desorption of CO_2 adsorbed on catalyst show two major peaks, one is located in the region of 350 ~ 450 K and the other in the region of 900 ~ 1075 K, which correspond to the weak basic sites and strong basic sites of the catalysts [35], respectively. The peaks appear at around 350 ~ 450 K might be attributed to the interaction between CO_2 and the weak basic sites [35], and stronger peak appearing at above 900 ~ 1075 K may result from the decomposition of the structural carbonate [36,37]. As shown in Fig. 4, with increasing the content of La, the peak at 900 ~ 1075 K became stronger. While for the CO_2 desorption peak at around 373 ~ 423 K, the 2 # La-modified TiO_2 sample show the highest intensity among the samples, indicating that appropriate content of La gives an optimized amount of weak basic sites. Such basic sites may enhance the adsorption of CO_2 on the catalyst and further promote the subsequent photoreduction of CO_2.

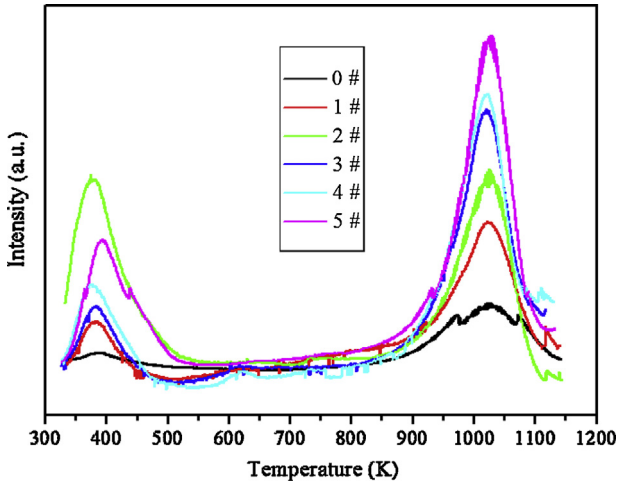

Fig. 4. CO_2-TPD profiles of 0 #, 1 #, 2 #, 3 #, 4 # and 5 # samples.

To investigate the surface chemical states and atomic concentration of La-modified TiO_2, the XPS spectra of La and Ti elements on the surface of La-modified TiO_2 nanoparticle samples (1–5 #) are shown in Fig. 5. It can be obtained from the XPS survey spectrum that 2 # and 5 # La-modified TiO_2 contain 4.1% and 8.4% La 3d, respectively (shown in Table 1). Regarding the La 3d core level spectra (Fig. 5a), it was observed that the splitting of the main peaks of La $3d_{5/2}$ and La $3d_{3/2}$ are at around 834.2 and 851.0 eV, respectively, and the shake-up satellite peaks of La $3d_{5/2}$ and La $3d_{3/2}$ are at 838.5 and 855.2 eV. In comparison with the bonding energy of pure La_2O_3 (834.9 eV) [38], the slight shift of La $3d_{5/2}$ (834.2 eV) to lower binding energy indicates the formation of La—O—Ti in the samples [27]. As shown in Fig. 5b, it can be seen that Ti 2p XPS spectra of La-modified TiO_2 is mainly composed of the main peaks of Ti $2p_{1/2}$ at 464.0 eV and Ti $2p_{3/2}$ at 458.2 eV, respectively, which shifts to a lower value in comparison with the reported result [39,40]. Therefore, it can be concluded that a tiny number of La atoms substitute the surface Ti atoms in the form of Ti—O—La.

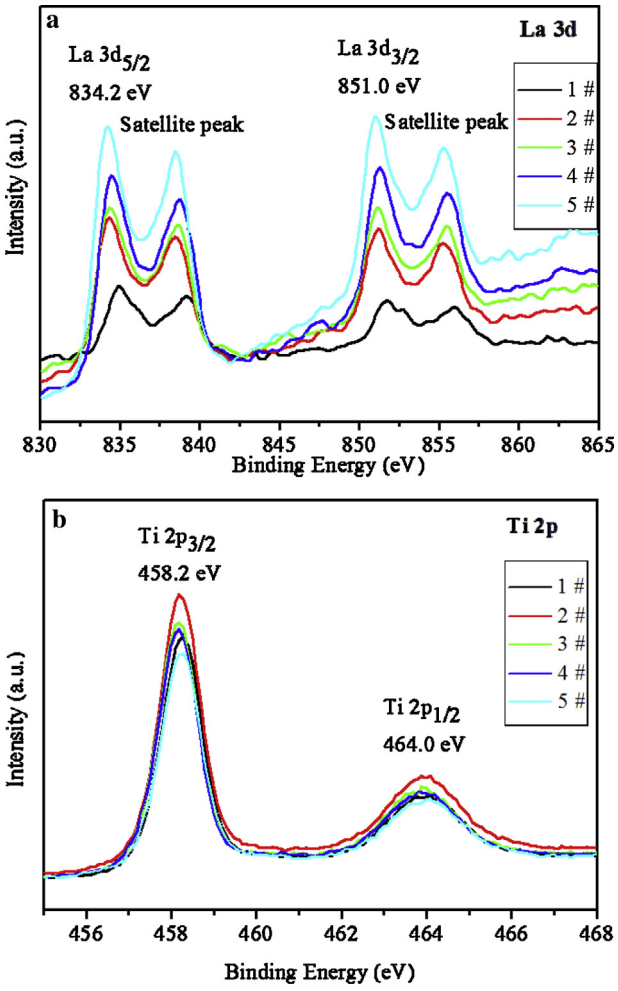

Fig. 5. XPS spectra for (a) La 3d of 1#, 2 #, 3#, 4#, and 5 # samples, (b) Ti 2p of 0 #, 1#, 2 #, 3#, 4#, and 5 # samples.

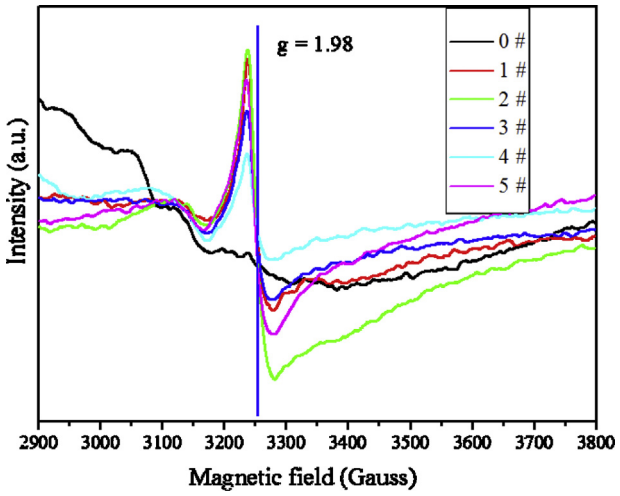

Fig. 6. EPR spectra for 0 #, 1 #, 2 #, 3 #, 4 # and 5 # samples.

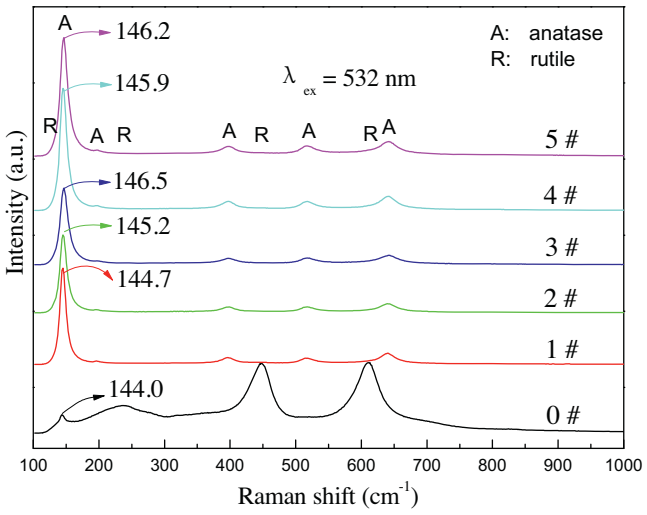

Fig. 7. Visible Raman spectra of 0 #, 1 #, 2 #, 3 #, 4 # and 5 # samples.

Electron paramagnetic resonance (EPR) measurements were further carried out on the as-prepared catalysts at room temperature. As shown in Fig. 6, all the La-modified TiO_2 samples gave rise to a strong EPR signal, while almost no signal was seen in the unmodified TiO_2 sample. The EPR spectra of La-modified TiO_2 samples show a paramagnetic signal centered around $g = 1.98$ (Fig. 6), it agrees very well with g values reported for Ti^{3+} ions [41]. It can also be seen from the Fig. 6, 2 # sample gives the highest intensity of EPR signal of Ti^{3+}, and further increasing the La loading from 2 # to 5 # did not lead to the enhancement of Ti^{3+}, which may because only a certain amount of La can modify the surface of TiO_2, and excessive La loading induces the accretion of La_2O_3 on the TiO_2 surface. DFT calculation on the spin density charge and Bader charge analysis of the La-modified TiO_2 further supports the formation of Ti^{3+} on the surface (Fig. S3). In combination this with the XRD patterns, XPS spectra, it can be concluded that La does not enter the bulk lattice of TiO_2, but it modifies TiO_2 in the form of Ti—O—La.

Fig. 7 shows the Raman spectra of 0 # sample and La-modified $TiO_{2(1\#-5\#)}$. From Fig. 7, it can be seen that the characteristic bands of rutile phase appear at 144, 235, 445, and 612 cm^{-1}, and the bands of anatase phase are at 143, 195, 395, 515, and 638 cm^{-1}. With the increase of La content, the intensities of the bands of rutile phase decrease, while those of anatase phase increase. Meanwhile, the increasing of La content also brings about a blue shift of the anatase peaks (from 143 cm^{-1} to present values), indicating the formation of oxygen vacancies [42], which could be due to the distortion of anatase crystalline lattice induced by La modification [43]. For La-modified TiO_2, the oxygen vacancies are prone to be formed because the chemical bond strength of La—O is stronger than the Ti—O [27]. However, excess loading of La (4 #) incurs a slight red shift of anatase peaks in comparison with that of 3 mol% (146.5 cm^{-1}) La-modified TiO_2, implying the decrease of oxygen vacancies, which could be attributed to excess of La_2O_3 covering on the surface of anatase TiO_2.

The oxygen vacancies are favorably generated on the La-modified TiO_2 surface can also be verified by the quantum calculation (Fig. 8 and Fig. S2). The formation energy of an oxygen vacancy on the surface of pure TiO_2 (Fig. 8b) from the (1 0 1) surface of anatase TiO_2 (Fig. 8a), and that of La-modified TiO_2 (Fig. 8d) from La-modified (1 0 1) surface of anatase TiO_2 (Fig. 8c) were calculated. And the oxygen vacancy formation energy was defined as:

$$E_{vac} = E(cell_{vac}) + 1/2E(O_2) - E(cell)$$

where $E(cell_{vac})$ and $E(cell)$ are the total energies of the optimized supercell with and without an oxygen vacancy, and $E(O_2)$ is the

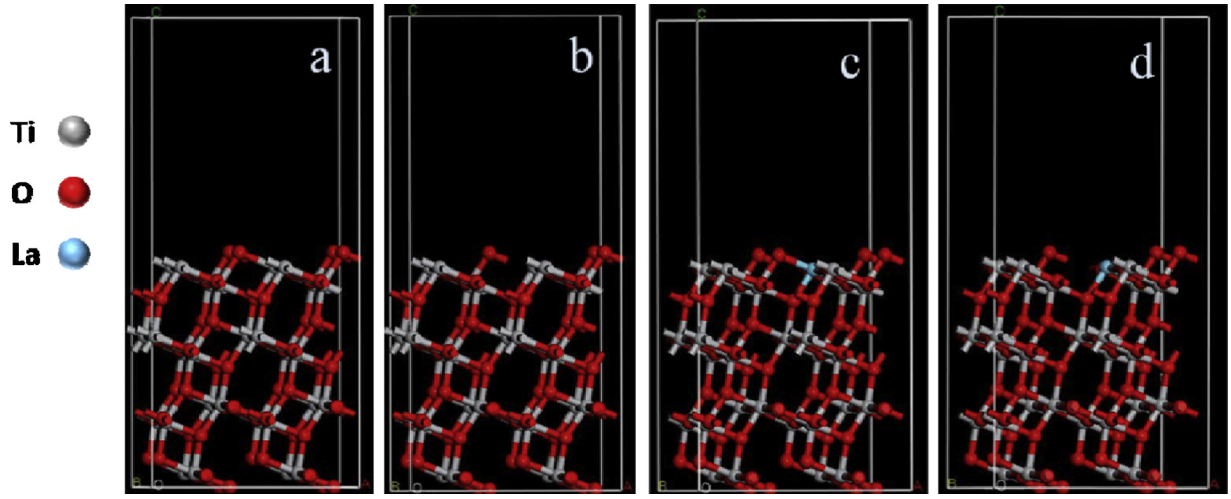

Fig. 8. Sketch of pure TiO_2 with a perfect surface (a) and pure TiO_2 with an imperfect surface with oxygen vacancies (b), the La-modified surface of TiO_2 (c), and the La-modified surface with oxygen vacancies (d) on the anatase TiO_2(1 0 1) surface. The gray, red, and blue balls denote Ti, O, and La atoms, respectively. (For interpretation of the references to colour in this figure legend, the reader is referred to the web version of this article.)

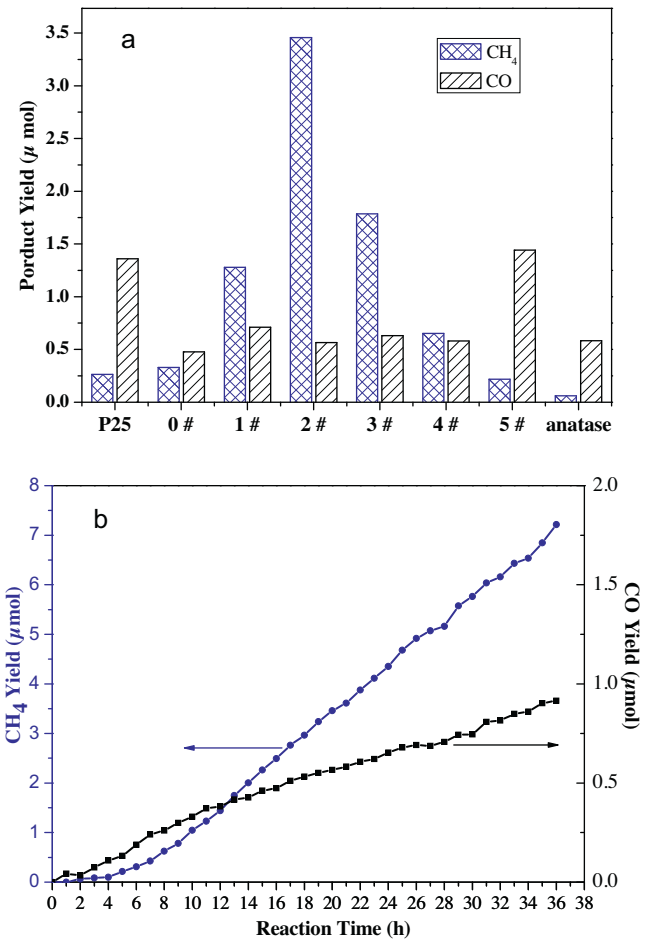

Fig. 9. Product yields of CO and CH_4 over (a) P25, anatase TiO_2 and 0 #, 1 #, 2 #, 3 #, 4 # and 5 # samples with irradiation time 20 h, (b) 2 # samples with irradiation time 36 h.

energy of free oxygen molecule in gas phase. A positive value of E_{vac} means that energy is needed to create the vacancy. The calculated result is that the formation energy of an oxygen vacancy on the La-modified TiO_2 surface (–0.72 eV) is lower than that formed on the pure TiO_2 surface (1.74 eV). In other words, the oxygen vacancies formed from the La-modified TiO_2 surface is much easier than that formed from the pure TiO_2 surface.

3.2. Photocatalytic performances

The photoreduction of CO_2 in the presence of water vapor was operated in a closed gas-circulation system, and the photocatalytic activities of all photocatalysts were measured under simulated solar irradiation Fig. 9a shows the yield of CO and CH_4 from CO_2 photoreduction using pure anatase, Degussa P25 and La-modified TiO_2 samples under UV–vis illumination for 20 h. Compared with the P25 and anatase, all the La-modified TiO_2 samples demonstrated enhanced CH_4 selectivity except for 5 # La-modified TiO_2 sample. For La-modified TiO_2 samples, the yield of CH_4 first increases and then decreases with the increasing of La content. Among the samples with different La contents, 2 # sample shows the highest yield of CH_4. In comparison with the yield of CH_4 of 0.264 μmol on TiO_2 (P25), 3.457 μmol of CH_4 was achieved on 2 # sample, showing a 13 times enhancement of CH_4 yield.

To confirm the present conversion is a photocatalytic reduction process, the reaction was performed in the absence of photocatalyst or light irradiation, and no reduced products were detected. In addition, when the reactor was filled with He (instead of CO_2) and H_2O vapor, no carbon-containing compounds were detected either. To further elucidate the origin of the CO and CH_4, the ^{13}C isotopic tracer experiments by GC–MS using $^{13}CO_2$ (Fig. S4) were conducted. The results show that the C in the photocatalytic products of CO and CH_4 is mainly from CO_2.

Based on the characterization and photocatalytic evaluation results, the increased formation of CH_4 on the as-prepared catalysts could be due to the following factors: (1) the introducing of La_2O_3 to the present catalysts could effectively adsorb CO_2 because of its basic characteristics. Such adsorption is of great importance for photoreduction of CO_2; (2) the surface modification of La exists in the form of Ti—O—La bond at the interface of La_2O_3 and TiO_2 (Fig. 10), and oxygen vacancies and Ti^{3+} are favorably generated on the surface of TiO_2. Consequently, the formed oxygen vacancies help to adsorb and dissociate H_2O, and the Ti^{3+} sites could bind CO_2 [44], both contributing to the subsequent photoreduction; (3) La_2O_3 on TiO_2 surfaces might capture the electrons and facilitate the separation of photogenerated electrons and holes, and Ti^{3+} also could separate electrons and holes, which is more effective than the sole electron trapping effect by TiO_2 alone. Specifically in photoreduction of CO_2 and H_2O, the formations of CO and CH_4 require two and eight electrons, respectively. For the La-modified TiO_2, a band gap of 3.0 eV with valence band edge at 2.4 eV and the conduction band edge of −0.6 eV vs. NHE (pH 7) was estimated [45] (Fig. 10). The reduction potential for the formations of CH_4 and CO are −0.24 eV and −0.52 eV, respectively [46]. So CH_4 will be favorably formed if there exists enough electrons and H^+. For the present catalysts, the synergistic effect between basic oxide La_2O_3, which enhances the adsorption of CO_2 molecules on the catalyst surface, and the formation of oxygen vacancies and Ti^{3+}, which supply enough H^+ and electron, result in the improvement of photocatalytic reduction of CO_2 to CH_4.

To investigate the photostability of as-prepared catalysts, the 2 # sample was selected to perform prolonged photoactivity reaction. As shown in Fig. 9b the yield of CO and CH_4 were increased continually with 36 h irradiation, indicating the good photostability of the photocatalyst.

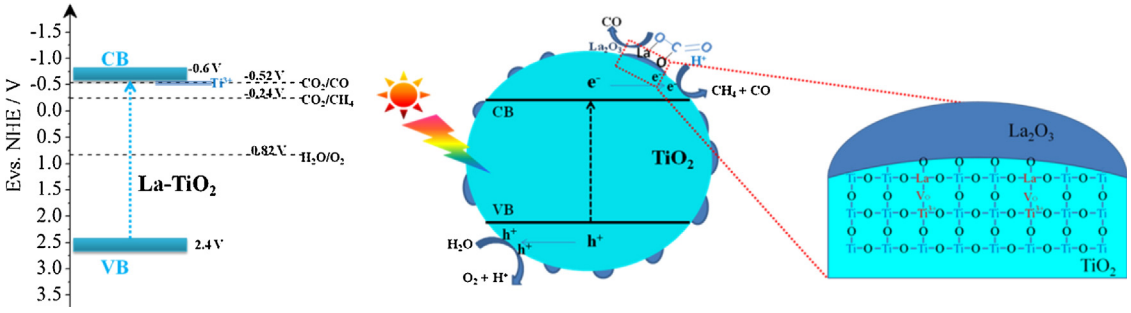

Fig. 10. Mechanism for the photoreduction of CO_2 with H_2O vapor over the La-modified TiO_2 photocatalyst.

4. Conclusions

Surface La-modified TiO_2 photocatalysts with different La amounts were prepared and tested for photocatalytic reduction of CO_2 in the presence of water vapor. The results showed that the La^{3+} was mostly uniformly dispersed onto TiO_2 in the form of La_2O_3 particles, and a handful of La atoms modify the surface of TiO_2 in the form of Ti—O—La. The introduction of La to the TiO_2 also promotes the formation of oxygen vacancies and Ti^{3+} onto the surface of TiO_2. Consequently, La-modified TiO_2 samples demonstrate the enhanced CH_4 selectivity, with a 13 times of CH_4 yield of that on the P25 reference sample. The significantly enhanced CH_4 selectivity on surface La-modified TiO_2 samples is mainly attributed to the synergistic effects of the highly dispersion of La_2O_3 and the formations of Ti^{3+} and oxygen vacancies on the adsorption of the CO_2 and H_2O as well as the separation of photo-generated electrons and holes. Such a La_2O_3-loaded TiO_2 catalyst with La surface modification helps to provide new insights into the design and development of highly efficient photocatalysts for photoreduction of CO_2 with H_2O vapor.

Acknowledgements

This work is financially supported by Prospect Oriented Foundation of China University of Petroleum, Beijing (Grant Nos.QZDX-2011-02, QZDX-2014-02), Beijing Nova Program (Grant No. Z11111005450000), Beijing Higher Education Young Elite Teacher Project (YETP0696), and Program for New Century Excellent Talents in University (NCET-11-0732).

Appendix A. Supplementary data

Supplementary data associated with this article can be found, in the online version, at http://dx.doi.org/10.1016/j.apcatb.2014.12.011.

References

[1] T. Inoue, A. Fujishima, S. Konishi, K. Honda, Nature 277 (1979) 637–638.
[2] S.C. Roy, O.K. Varghese, M. Paulose, C.A. Grimes, ACS Nano 4 (2010) 1259–1278.
[3] A. Dhakshinamoorthy, S. Navalon, A. Corma, H. Garcia, Energy Environ. Sci. 5 (2012) 9217–9233.
[4] K. Mori, H. Yamashita, M. Anpo, RSC Adv. 2 (2012) 3165–3172.
[5] I.H. Tseng, W.C. Chang, J.C.S. Wu, Appl. Catal. B: Environ. 37 (2002) 37–48.
[6] Y. Li, W.N. Wang, Z. Zhan, M.H. Woo, C.Y. Wu, P. Biswas, Appl. Catal. B: Environ. 100 (2010) 386–392.
[7] N.L. Wu, M.S. Lee, Int. J. Hydrogen Energy 29 (2004) 1601–1605.
[8] I.H. Tseng, W.C. Chang, J.C.S. Wu, Appl. Catal. B: Environ. 37 (2002) 37–48.
[9] V.P. Indrakanti, J.D. Kubicki, H.H. Schobert, Energy Environ. Sci. 2 (2009) 745–758.
[10] W. Balcerski, S.Y. Ryu, M.R. Hoffmann, J. Phys. Chem. C 111 (2007) 15357–15362.
[11] T. Yui, A. Kan, C. Saitoh, K. Koike, T. Ibusuki, O. Ishitani, ACS Appl. Mater. Interfaces 3 (2011) 2594–2600.
[12] W.N. Wang, W.J. An, B. Ramalingam, S. Mukherjee, D.M. Niedzwiedzki, S. Gangopadhyay, P. Biswas, J. Am. Chem. Soc. 134 (2012) 11276–11281.
[13] O.K. Varghese, M. Paulose, T.J. LaTempa, C.A. Grimes, Nano Lett. 9 (2009) 731–737.
[14] L. Collado, P. Jana, B. Sierra, J.M. Coronado, P. Pizarro, D.P. Serrano, V.A. de la Peña O'shea, Chem. Eng. J. 224 (2013) 128–135.
[15] L.J. Liu, F. Gao, H.L. Zhao, Y. Li, Appl. Catal. B: Environ. 134–135 (2013) 349–358.
[16] Q.G. Zhai, S.J. Xie, W.Q. Fan, Q.H. Zhang, Y. Wang, W.P. Deng, Y. Wang, Angew. Chem. Int. Ed. 52 (2013) 5776–5779.
[17] Y.G. Wang, B. Li, C.L. Zhang, L.F. Cui, S.F. Kang, X. Li, L.H. Zhou, Appl. Catal. B: Environ. 130–131 (2013) 277–284.
[18] J.Q. Jiao, Y.C. Wei, Z. Zhao, J. Liu, J.M. Li, A.J. Duan, G.Y. Jiang, Ind. Eng. Chem. Res. 53 (2014) 17345–17354.
[19] L.J. Liu, C.Y. Zhao, H.L. Zhao, D. Pitts, Y. Li, Chem. Commun. 49 (2013) 3664–3666.
[20] S.J. Xie, Y. Wang, Q.H. Zhang, W.Q. Fan, W.P. Deng, Y. Wang, Chem. Commun. 49 (2013) 2451–2453.
[21] O.K. Varghese, M. Paulose, T.J. LaTempa, C.A. Grimes, Nano Lett. 9 (2009) 731–737.
[22] S. Zhou, Y. Liu, J.M. Li, Y.J. Wang, G.Y. Jiang, Z. Zhao, D.X. Wang, A.J. Duan, J. Liu, Y.C. Wei, Appl. Catal. B: Environ. 158–159 (2014) 20–29.
[23] Q.Y. Zhang, Y. Li, E.A. Ackerman, M. Gajdardziska-Josifovska, H.L. Li, Appl. Catal. A: Gen. 400 (2011) 195–202.
[24] U. Diebold, Surf. Sci. Rep. 48 (2003) 53–229.
[25] K. Teramura, T. Tanaka, H. Ishikawa, Y. Kohno, T. Funabiki, J. Phys. Chem. B 108 (2004) 346–354.
[26] A.W. Xu, Y. Gao, H.Q. Liu, J. Catal. 207 (2002) 151–157.
[27] J.Y. Zhang, Z.Y. Zhao, X.Y. Wang, T. Yu, J. Guan, Z.T. Yu, Z.S. Li, Z.G. Zou, J. Phys. Chem. C 114 (2010) 18396–18400.
[28] L. Matějová, K. Kočí, M. Reli, L. Čapek, A. Hospodková, P. Peikertová, Z. Matěj, L. Obalová, A. Wach, P. Kuśtrowski, A. Kotarba, Appl. Catal. B: Environ. 152–153 (2014) 172–183.
[29] L.Q. Jing, X.J. Sun, B.F. Xin, B.Q. Wang, W.M. Cai, H.G. Fu, J. Solid State Chem. 177 (2004) 3375–3382.
[30] G. Kresse, J. Furthmüller, Phys. Rev. B 54 (1996) 11169–11186.
[31] P.E. Blöchl, Phys. Rev. B 50 (1994) 17953–17979.
[32] J.P. Perdew, K. Burke, M. Ernzerhof, Phys. Rev. Lett. 77 (1996) 3865–3868.
[33] T. Sreethawong, Y. Suzuki, S. Yoshikawa, J. Solid State Chem. 178 (2005) 329–338.
[34] J. Zhang, M.J. Li, Z.C. Feng, J. Chen, C. Li, J. Phys. Chem. B 110 (2006) 927–935.
[35] R.L. Song, D.M. Tong, J.Q. Tang, C.W. Hu, Energy Fuels 25 (2011) 2679–2686.
[36] B.M. Faroldi, J.F. Múnera, L.M. Cornaglia, Appl. Catal. B: Environ. 150–151 (2014) 126–137.
[37] S. Sato, R. Takahashi, M. Kobune, H. Gotoh, Appl. Catal. A: Gen. 356 (2009) 57–63.
[38] T.H. Fleisch, R.F. Hicks, A.T. Bell, J. Catal. 87 (1984) 398–413.
[39] B. Erdem, R.A. Hunsicker, G.W. Simmons, E.D. Sudol, V.L. Dimonie, M.S. El-Aasser, Langmuir 17 (2001) 2664–2669.
[40] Q.Y. Zhang, T.T. Gao, J.M. Andino, Y. Li, Appl. Catal. B: Environ. 123–124 (2012) 257–264.
[41] M. Anpo, T. Shima, T. Fujii, S. Suzuki, M. Che, Chem. Lett. 10 (1987) 1997–2000.
[42] J.C. Parker, R.W. Siegel, Appl. Phys. Lett. 57 (1990) 943–945.
[43] Y.N. Huo, J. Zhu, J.X. Li, G.S. Li, H.X. Li, J. Mol. Catal. A: Chem. 278 (2007) 237–243.
[44] M. Manzanares, C. Fàbrega, J.O. Ossó, L.F. Vega, T. Andreu, J.R. Morantea, Appl. Catal. B: Environ. 150–151 (2014) 57–62.
[45] A. Fujishima, X.T. Zhang, D.A. Tryk, Surf. Sci. Rep. 63 (2008) 515–582.
[46] G.A. Olah, G.K.S. Prakash, A. Goeppert, J. Am. Chem. Soc. 133 (2011) 12881–12898.